Role of adhesive interlayer in transverse fracture of brittle layer structures

Herzl Chai
Department of Solid Mechanics, Materials and Structures Faculty of Engineering, Tel Aviv University, Israel 69978

Brian Lawn
Materials Science and Engineering Laboratory, National Institute of Standards and Technology, Gaithersburg, Maryland 20899

(Received 2 December 1999; accepted 31 January 2000)

The role of a soft adhesive interlayer in determining critical conditions for fracture in brittle layer structures from indentation with hard spheres is investigated. A model transparent trilayer system consisting of a glass plate overlayer (thickness range 80 μm to 2 mm) joined to a glass plate underlayer (thickness 5.6 mm) by an epoxy adhesive (thickness range 5 μm to 8 mm), loaded at its top surface with a hard tungsten carbide sphere (radius 3.96 mm), facilitates *in situ* observations of the crack initiation and propagation. Whereas in bulk glass fracture occurs by inner Hertzian cone cracking immediately outside the contact circle, the soft adhesive allows the overlayer glass plate to flex, initiating additional transverse fracture modes within the overlayer: downward-extending outer ring cracks at the top glass surface well outside the contact, and upward-extending radial cracks at the bottom glass surface (i.e., at the glass/adhesive interface) on median planes containing the contact axis. The top and bottom surfaces of the glass overlayers are given selective prebonding abrasion treatments to ensure uniform flaw states, so as to enable accurate comparisons between crack initiation conditions. The adhesive bonding is strong enough to preclude delamination in our layer system. Of the three transverse crack systems, the subsurface radials generates most easily in systems with large adhesive thicknesses (and smaller overlayer thicknesses). Semi-empirical relations are specified for the dependence of the critical loads for radial and ring cracking on adhesive as well as overlayer thickness, based on the assumption that crack initiation occurs when the maximum tensile stresses in the flexing glass plate exceed the bulk strength of the (abraded) glass. Coupled with the traditional "Auerbach's law" for cone crack initiation, these relations afford a basis for the construction of simple design diagrams for brittle layer systems joined by adhesives.

I. INTRODUCTION

Brittle layers can be made damage tolerant by joining them together into laminate structures with a weak adhesive interphase.[1–4] Practical examples are seashells, natural teeth and dental crowns, car windscreens, and some thermal barrier coatings. The brittle layers afford stiffness, wear resistance and durability; the compliant interlayer provides damage tolerance, by redistributing stresses, and confining fractures within individual brittle layers. The adhesive needs to be weak enough to prevent cracks from penetrating into adjacent layers but strong enough to preclude delamination failures.

The damage tolerance properties of such stiff-layer/soft-foundation structures are especially conspicuous in concentrated loading configurations, e.g., indentation with hard spheres, projectile impacts. In such cases the outer brittle layers are subject to transverse (through-thickness) cracking. Such cracking has been well documented in many ceramic-based layer and coating systems on soft supporting substrates, from examination of sections through indentation sites.[5–17] Two new contact-induced transverse crack systems have been identified in these studies: surface circumferential ring cracks that initiate at the top surface well outside the contact circle (distinct from conventional cone cracks that occur just outside the contact in monolithic materials); and subsurface median–radial cracks that initiate at the bottom surface of the overlayer, i.e., at the interface with the soft support. Normal stresses across the interface plane are compressive below the contact, so delamination cracks

 © 2000 Materials Research Society

do not usually occur in such systems, provided the bonding between layers is sufficiently strong and the soft layers do not undergo extensive yield.[18]

However, "post-mortem" section studies are not amenable to straightforward measurements of critical initiation loads, nor to determining the ensuing (three-dimensional) crack geometries, especially of the subsurface cracks. Such characteristics of the fracture pattern are much more easily studied in transparent layer systems, by *in situ* observation during actual contact testing.[19] In this paper we use such a model system to examine the role of an adjoining adhesive in the contact fracture properties of brittle laminates. We construct model trilayers consisting of glass plate overlayers (thickness range 80 μm to 2 mm) glued to thick glass underlayers (5.6 mm) with epoxy adhesive (thickness range 5 μm to 8 mm). The appeal of using like materials on either side of the interface is that the incidence of any fracture modes other than conventional cone cracking can be unequivocally attributed to the influence of the adhesive. Load is applied via a hard tungsten carbide (WC) sphere (radius 3.96 mm), and the onset and evolution of each crack is monitored using an *in situ* low-power microscope arrangement. We shall demonstrate that the presence of the adhesive interlayer can have a profound influence on the critical loads as well as on the types of transverse crack, even for adhesive thicknesses as small as 5 μm. From simple empirical relations for the critical loads as functions of adhesive and glass overlayer thicknesses, we shall construct design diagrams for optimizing resistance to fracture. The high stability of the transverse cracks, once formed, will be duly noted, but deferred to another study for more detailed analysis.

II. EXPERIMENTAL PROCEDURE

We construct a model trilayer system from transparent brittle plates to enable direct *in situ* viewing of coating fracture during indentation testing, with upper layer thickness d and adhesive thickness h, subject to contact loading with a sphere of radius r at load P, Fig. 1. The upper plate in contact with the indenter is designated the "overlayer," and the lower support plate ($\gg d$) the "underlayer."

Soda-lime window glass slabs 75 × 18 × 5.6 mm were used for the underlayer plates. Slabs for the overlayer plates were ground to prescribed thicknesses within the range $d = 80$ μm to 2 mm and polished to 1 μm diamond paste. Chemical etching in a solution of 12% hydorfluoric (HF) acid for up to 10 min was used as a means of thinning at the lower end of the thickness range and also of preparing selected surfaces in a relatively flaw-free state. To obtain reproducible critical load data, selective abrasion of the top or bottom overlayer glass surfaces using a slurry of 600 SiC grit was employed.

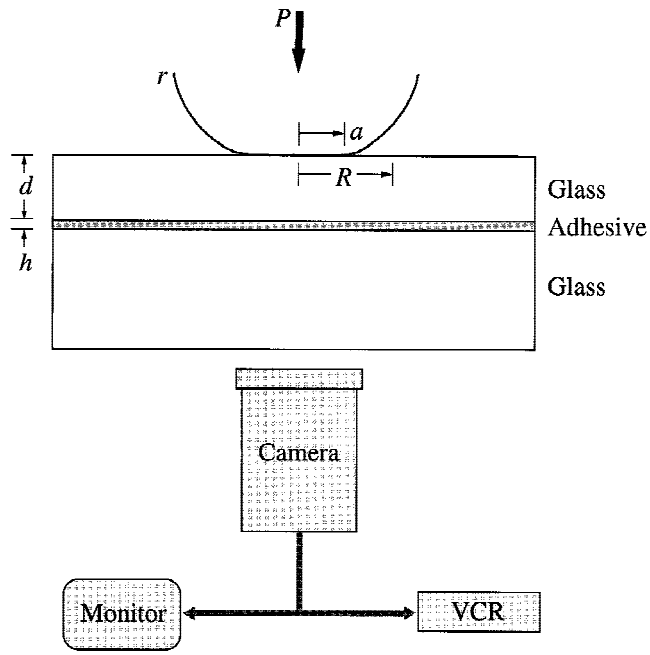

FIG. 1. Schematic of glass/adhesive/glass trilayer system, overlayer glass thickness d and adhesive thickness h, for indentation with sphere of radius r at load P (underlayer glass thickness $\gg d$), contact radius a and radial direction R indicated. Transverse crack systems generated in the brittle overlayer in the vicinity of the contact are viewed by a subsurface camera arrangement.

An epoxy adhesive (Harcos Chemicals, Bellesville, NJ) was used to bond the upper and lower glass plates together. This was done at room temperature, under light pressure. This bonding procedure eliminated the likelihood of significant residual stresses in the glass layers. The thicknesses of the final adhesive layer were controlled by inserting metal shims at the specimen interface ends. In some specimens the shims at opposite ends were of different thickness, producing an adhesive joint with graded thickness to enable more rapid data accumulation, but never with adjacent glass surfaces inclined at more than 0.5°. Thicknesses over a range $h = 5$ μm to 0.5 mm were prepared in this way. Thicker bonds, 0.5 mm up to 8 mm, were prepared by filling part of the gap with thin polycarbonate slabs, again with epoxy adhesive as a bonding agent. As indicated in our previous paper, the properties of the polycarbonate are sufficiently similar to that of the adhesive as to produce indistinguishable fracture data.[19] In all cases the top surfaces were carefully aligned normal to the load axis.

Indentation tests were conducted on the glass overlayer surfaces with WC spheres of radius $r = 3.96$ mm, in a screw-driven testing machine (Instron 4501, Instron Corp, Canton, MA), in air, as before.[19] These tests were made at constant crosshead speed such that transverse cracks initiated in the glass coatings within 1 min or so. The subsurface contact regions in the coatings were observed *in situ* using a Questar telescope (Questar, New

Hope, PA), either from below using a mirror to redirect the light source or directly through the side surface; in the former case the top contact surface was precoated with a gold film to enhance reflection. The indentation crack evolution was observed directly on a monitor and recorded on a video recorder unit, with provision for on-screen recording of indentation load. Critical loads to initiate each fracture mode were thus measured.

III. RESULTS

A. Crack morphology

Representative examples of the crack morphologies in the glass overlayer, photographed *in situ* from below the contact during loading, are shown in Figs. 2 and 3. Confirmation of the origin of cracking, i.e., bottom or top surface, was obtained from subsidiary side viewing experiments.

Figure 2 illustrates the crack pattern for a specimen in which the *bottom* surface of the overlayer glass plate was abraded prior to bonding to the underlayer. Radial cracks generate immediately below the contact (central bright spot), at the bottom surface of the overlayer. The sequence shows the crack development at increasing load for a glass thickness $d = 310$ μm and adhesive thickness $h = 360$ μm: (a) load $P = 32$ N, just above the threshold load, one set of diametrically opposed subsurface radial cracks; (b) at $P = 68$ N, two sets of radials, which expand more or less equally; (c) at $P = 96$ N, an outer ring crack originating from the top surface, well outside the contact circle. The radial cracks extend laterally outward, sometimes to the edges of the specimen, but remain subsurface without penetrating through the thickness to the top of the overlayer, except at very high loads.[12,19] Note that the ring crack in Fig. 2(c) is not perfectly axisymmetric and occurs near the periphery of the preceding radials, suggesting significant crack–crack interactions.

Figure 3 illustrates analogous crack patterns for specimens in which the *top* surfaces of overlayer glass plate were abraded. In these cases ring cracks generate at the top surface outside the contact circles. The micrographs show ring crack patterns for two adhesive thicknesses, at fixed glass thickness $d = 310$ μm, for loads at or just above threshold: (a) "thin" adhesive, $h = 26$ μm, a conventional "inner" cone crack with surface trace R_0 just outside the contact circle a, $R_0/a = 1.5$; (b) "thick" adhesive, $h = 360$ μm, a much wider "outer" ring crack at several times the contact radius, $R_0/a = 6$. In these cases the outer ring crack has near-axisymmetry [cf. Fig. 2(c)].

A normalized plot of ring-crack surface trace R_0 as a function of adhesive thickness h, relative to overlayer plate thickness d, is given in Fig. 4 for specimens with top surfaces abraded. In this plot we arbitrarily distinguish

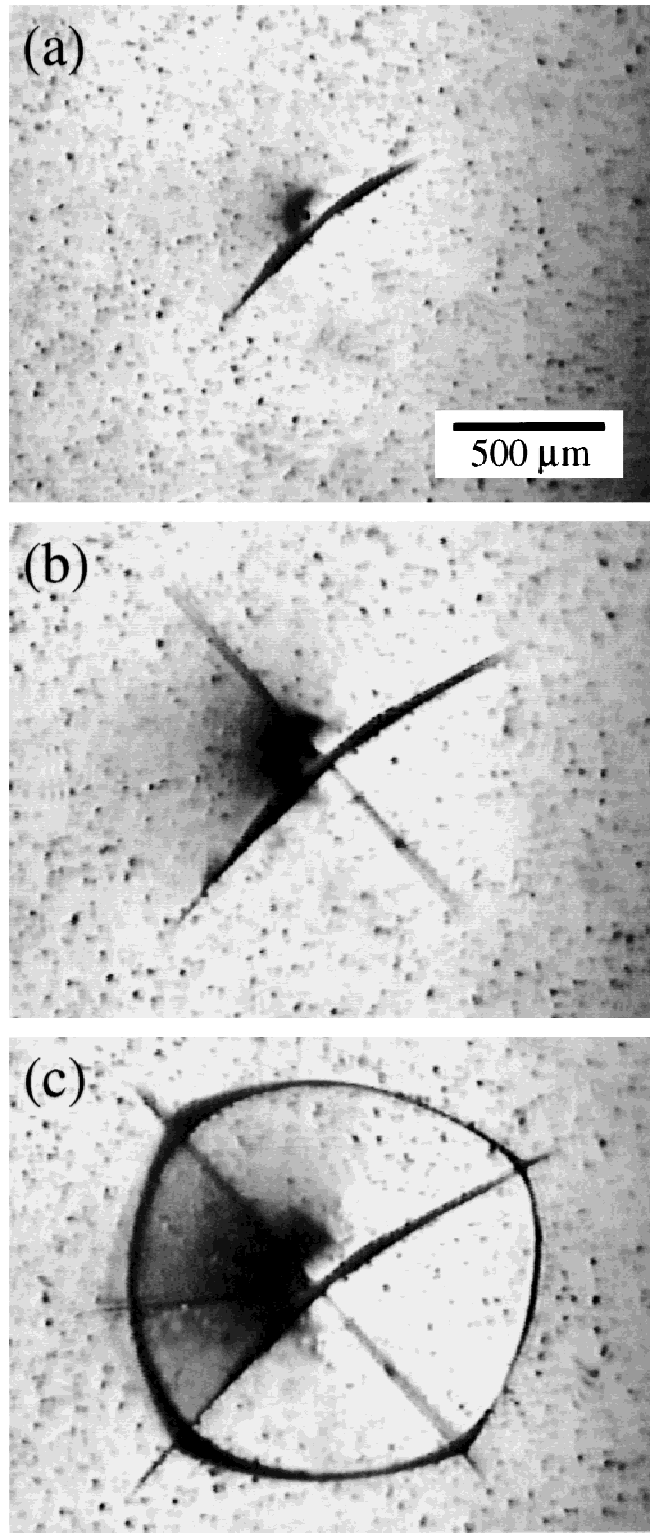

FIG. 2. *In situ* micrographs of crack evolution in overlayer soda-lime glass plates of thickness $d = 310$ μm, *bottom* surfaces abraded, bonded with adhesive of thickness $h = 360$ μm to like underlayer soda-lime glass plates of fixed thickness 5.6 mm. Indentation with WC sphere radius $r = 3.96$ mm, contact loads: (a) $P = 32$ N, (b) $P = 68$ N, (c) $P = 96$ N. Abrasion flaws and contact zone (central bright spot) are visible.

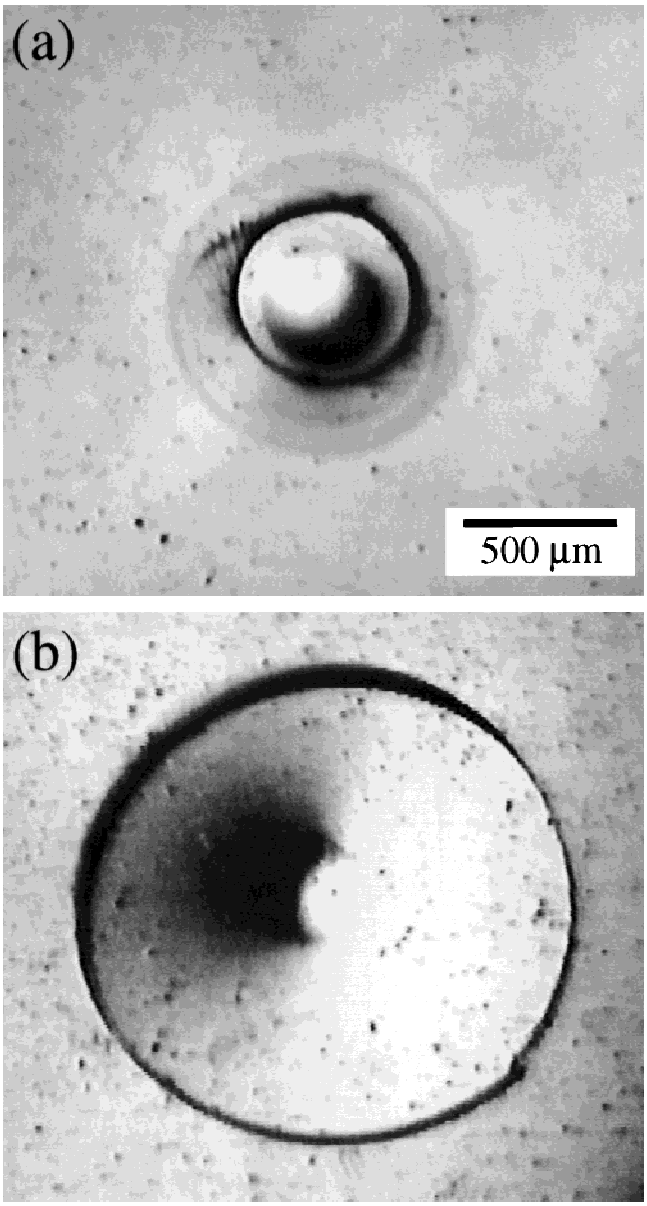

FIG. 3. *In situ* micrographs of crack evolution in overlayer soda-lime glass plates of thickness $d = 310$ μm, *top* surfaces abraded, bonded with adhesive to like underlayer soda-lime glass plates of fixed thickness 5.6 mm, from indentation with WC sphere radius $r = 3.96$ mm, adhesive thickness and contact loads: (a) $h = 26$ μm, $P = 199$ N; (b) $h = 360$ μm, $P = 137$ N. Abrasion flaws and contact zone (central bright spot) are visible.

inner rings (unfilled symbols) and outer rings (filled symbols) by the condition $R_0/a = 2$, using surface trace measurements from micrographs (e.g., Fig. 3). Data are shown for selected values of d. The vertical dashed line at $h_*/d \approx 0.2$ delineates the transition from inner cone to outer ring, most clearly at larger d values—note that some of the data overlap this condition somewhat, so the condition $h_*/d \approx 0.2$ is at best an approximation. The solid curve is an empirical universal fit to the outer ring data—this curve tends asymptotically to a limit $R_0/d \approx 4$ at $h \gg h_*$ for infinite adhesive substrates, confirming a certain self-similarity in the outer ring geometry.[19]

All three transverse cracks, once initiated, are highly stable. They grow and proliferate with increasing load, and ultimately interact with secondary cracks [e.g., Fig. 2(c)].[19] Considerable load increase beyond the threshold is required to cause general overlayer failure by penetration of one or other cracks through the layer, with consequent delamination and spalling.

B. Critical loads

Critical loads for radial cracking as a function of adhesive thickness, $P_{rad}(h)$, are plotted for specified values of d in Fig. 5, for specimens with bottom surfaces abraded. Each data point represents an individual radial crack initiation event. Solid curves are theoretical fits (see Sec. IV). Increasing d increases P_{rad} at any specified h, as documented in our earlier study of bilayer glass coatings on semi-infinite polymer substrates.[19] For any given d, P_{rad} declines with increasing h, tending asymptotically to the bilayer limit at $h \rightarrow \infty$.[19]

An analogous plot of critical load data $P_{ring}(h)$ for specified values of d is shown in Fig. 6. Initially, at $h < h_* \approx 0.2d$ (vertical dashed lines), the ring cracks develop as inner cones ($R_0 < 2a$), designated by the unfilled symbols. The horizontal dashed line indicates the critical load P_{cone} for monolithic glass.[19] In this region, measured values of P_{cone} are quite insensitive to h, as well as to d, although those for larger d do tend markedly upward as h approaches h_*. At $h > h_*$, the nature of cracking changes abruptly to outer ring ($R_0 > 2a$), designated by the filled symbols. Again, solid curves are theoretical fits to the data (Sec. IV). In this region, $P_{ring}(h)$ follows the same trend as the data for $P_{rad}(h)$ in Fig. 5, albeit at higher P values; i.e., increasing with d at any given h, and declining with h at any given d.

IV. ANALYSIS

Analytical solutions for tensile stresses in general trilayer systems of the kind depicted in Fig. 1 are unavailable. Arguably the closest is a solution $\sigma \propto (P/d^2) \log(Ed^3/ka^4)$ for the stresses in an elastic plate of modulus E center-loaded over contact radius a on a soft semi-infinite support of foundation "stiffness" k.[20] In our preceding analysis of bilayer glass coatings on soft polymer substrates[19] we used FEM to compute tensile stresses in the glass, and thence to confirm that critical loads $P_{rad}(d)$ and $P_{ring}(d)$ are consistent with the assumption that crack initiation occurs when and where these maximum tensile stresses exceed the bulk strength ($\sigma_F = 110 \pm 5$ MPa) of the (abraded) glass.[19] This assumption

was substantiated by the similarity between the far-contact tensile stress field ($R \gg a$, Fig. 1) in the glass coatings in our system and in flexing plates of the kind used to measure strengths of brittle materials. From that study, a result P_{rad} (or P_{ring}) $\propto \sigma_F d^{\beta}$ was derived from fits to the bilayer data, with $\beta \approx 1.75$. Here we adopt a simple approach and use an empirical modification to allow for the effect of adhesive thickness on the critical conditions.

It should be reiterated that previous studies have shown that the validity of a simple critical stress criterion for crack initiation does not extend to the near-contact field ($R \approx a$, Fig. 1) where inner cone cracks initiate, owing to inordinately high stress gradients in this region.[21–23] This breakdown of a critical stress concept manifests itself as an altogether different functional dependence of P_{cone} on test and material variables, somewhat independent of d in bilayer systems.[19]

A. Radial cracks

Assume that only the bottom surface of the glass overlayer contains flaws, so that subsurface radial cracks form before rings. To allow for the influence of finite adhesive thickness h, we modify the empirical critical load relation from our earlier study of brittle coatings on thick soft substrates[19]:

$$P_{rad} = B_{rad}\sigma_F d^{\beta}\,[1 + C(d/h)^{\gamma}] \quad , \qquad (1)$$

with γ an exponent, B_{rad} (dimensions length$^{2-\beta}$) and C (dimensionless) coefficients. Note that the modifying term in the square brackets reduces to unity in the limit $h = \infty$, so that Eq. (1) reduces to the bilayer result, as required. Note also that P_{rad} is independent of r, reflecting the far-field nature of this solution. Imposing $\sigma_F = 110 \pm 5$ MPa (above), we obtain best-fit parameters $\beta =$

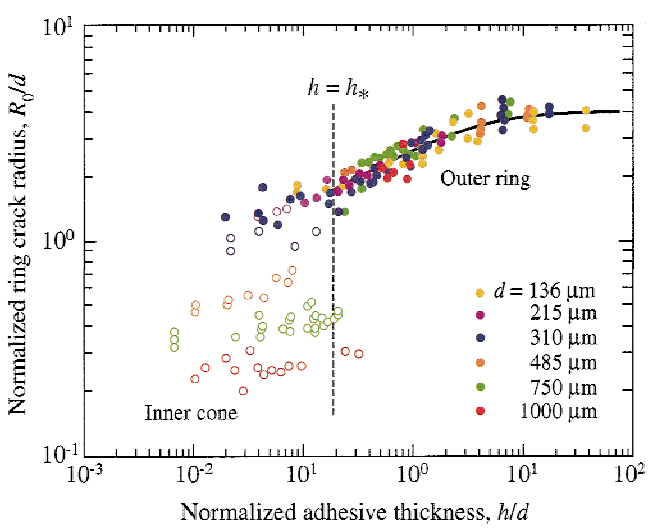

FIG. 4. Surface crack radius R_0 for ring cracks in overlayer soda-lime glass plates, *top* surfaces abraded, bonded with adhesive of thickness h to like glass underlayers of fixed thickness 5.6 mm. Data normalized to plate thickness d. WC indenter radius $r = 3.96$ mm. Cracks undergo transition from inner ring (cone) (unfilled symbols) to outer ring (filled symbols) at $h = h_* \approx 0.2d$. Solid curve is empirical fit.

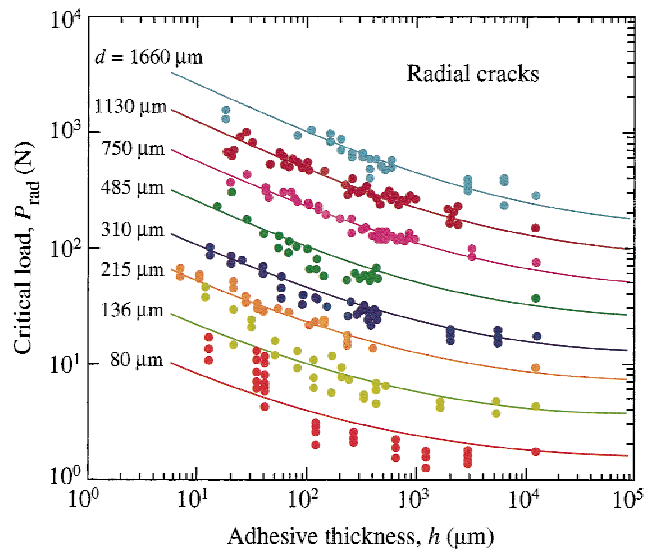

FIG. 5. Critical loads P_{rad} to initiate radial cracks at bottom surface of overlayer glass plate bonded to underlayer glass plate with adhesive of thickness h, for upper plate thicknesses d indicated. Data points are experimental results for specimens with bottom surface of overlayer abraded, WC indenter radius $r = 3.96$ mm. Solid curves are theoretical fits.

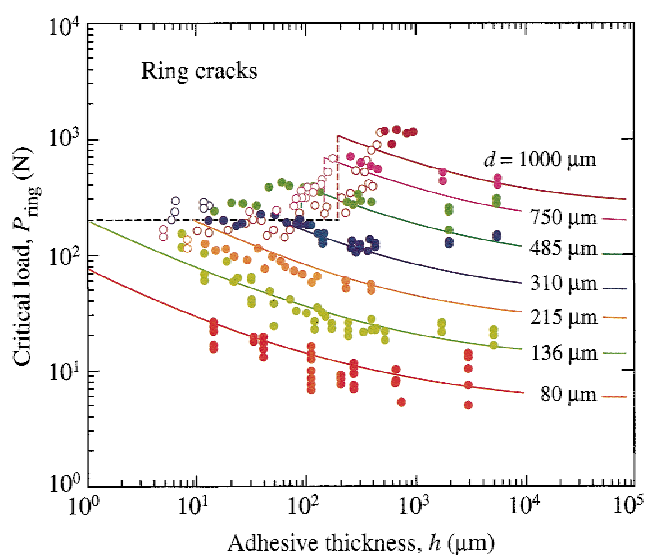

FIG. 6. Critical loads P_{ring} to initiate ring cracks at top surface of overlayer glass plate bonded to underlayer glass plate with adhesive of thickness h, for upper plate thicknesses d indicated. Data points are experimental results for specimens with top surface of overlayer abraded, WC indenter radius $r = 3.96$ mm: unfilled symbols represent inner cone cracks, and filled symbols outer ring cracks. Horizontal dashed line indicates critical load for cone cracking in monolithic glass, vertical dashed lines indicate transition adhesive thickness $h = h_*$ (Fig. 4). Solid curves are theoretical fits.

1.49, $B_{rad} = 0.018\ m^{2-\beta}$, $\gamma = 0.45$ and $C = 1.73$ for the data in Fig. 5. The solid curves are regenerations from Eq. (1) using these parameters (*cf.* $\beta \approx 1.75$ obtained for the glass-plate/polycarbonate-substrate thick bilayer system in our earlier study).[19]

B. Ring cracks

Now assume that only the top surface of the contacted glass layer contains flaws, so that either outer ring cracks ($h > h_*$) or inner surface cone cracks ($h < h_*$) form before radials. Since the outer ring cracks are assumed to form in the same linear far-field flexure stress fields as do the radials, we may simply replace B_{rad} in Eq. (1) with B_{ring}:

$$P_{ring} = B_{ring}\sigma_F d^{\beta}\,[1 + C(d/h)^{\gamma}], \qquad (h > h_*) \quad . \qquad (2)$$

Note again that P_{ring} is independent of r. The solid curves through the outer-ring data in Fig. 6 are generated using the same values of β, γ and C from the preceding radial data fit, with the single adjustment $B_{ring} = 0.065\ m^{\beta-2}$ to provide a best fit. Note that $B_{ring} > B_{rad}$, signifying a lower stress intensity maximum at the location of the ring crack relative to the radial crack.

As mentioned above, one cannot assume a simple critical stress criterion for initiation of the inner cone cracks. Notwithstanding the slight dependence on h apparent in the data in Fig. 6, the critical loads for cone cracks may be represented to first approximation by Auerbach's law for monolithic solids:[21–23]

$$P_{cone} = ArG_c, \qquad (h < h_*) \qquad (3)$$

with G_c the crack resistance and A Auerbach's constant (dimensionless, dependent on relative elastic properties of the indenter and specimen). Note P_{cone} in Eq. (3) is independent of d, reflecting a near-field solution. For $r = 3.96$ mm, taking $P_{cone} = 210$ N (horizontal dashed line in Fig. 6) and $G_c = 7.7\ J.m^{-2}$ for soda-lime glass,[24] we determine $A = 6.9 \times 10^3$.

We now have the basis for predicting critical loads for any specifiable adhesive layer thickness h and glass overlayer thickness d, and hence for designing interlayer structures for specific applications.

V. DISCUSSION

This study has examined the influence of an adhesive layer on contact fracture modes in multilayer systems. Specifically, we have considered a simple trilayer system with like glass sandwiching plates bonded by an epoxy adhesive, covering a broad range of layer thicknesses (adhesive, 5 μm to 8 mm; overlayer glass, 80 μm to 2 mm). We have chosen transparent materials to facilitate data acquisition using *in situ* observations during contact with sphere indenters on the overlayer surface, with a large interlayer modulus mismatch to embrace a diversity of fracture modes. Apart from traditional cone cracking at the top surface, other transverse cracks, i.e., subsurface radials and top surface outer rings, are generated. Such cracks are not ordinarily observed in monoliths. [An exception in monoliths occurs in contacts with sharp (e.g., Vickers) indenters, where intense quasiplasticity fields generate their own radial cracks.[25,26]] In our material system, the radial cracks initiate at relatively low critical loads and so represent an especially dangerous form of damage. These subsurface cracks may pass unnoticed in routine surface inspections of damaged coating layers, particularly in opaque materials. The extent of the influence of thickness of an intervening adhesive layer on the critical fracture conditions is illustrated in Fig. 5, where an increase in h from 10 μm to 10 mm diminishes the critical load P_{rad} by a factor of about 5 in our glass/adhesive system.

Our analysis in Sec. IV provides a basis for the construction of "universal" design diagrams for any given trilayer system subject to damage from blunt contacts (Fig. 1). Figure 7 is a plot of normalized critical loads $P_C/B_{rad}\,\sigma_F d^{\beta}$ as a function of normalized adhesive thickness h/d, in accordance with Eqs. (1) and (2) for radial and outer ring cracks. The curve for each of these two crack systems is universal for all h, d, and r. The horizontal line representing Eq. (3) for inner cone cracks, on the other hand, is dependent on r and d: here we arbitrarily plot this line for $P_{cone}/P_{rad}(h = \infty) = ArG_c/B_{rad}\sigma_F d^{\beta} = 8$. This plot maps out different damage zones: A, no cracks, safe zone (all h, $P < P_{cone}$, $P < P_{rad}$); B, inner rings (cone cracks), no radials ($h < h_*$, $P_{cone} < P$

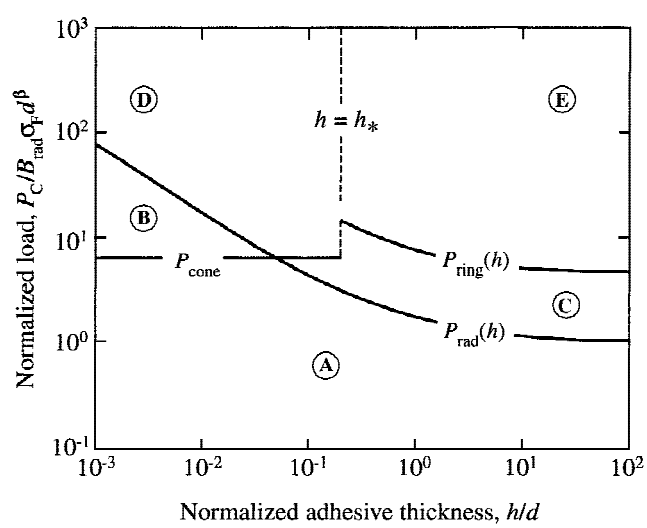

FIG. 7. Design diagram, showing critical loads P_{cone} = constant, and $P_{rad}(h)$, $P_{ring}(h)$. Plots are made "universal" by normalizing loads to quantity $B_{rad}\sigma_F d^{\beta}$ in Eq. 1, and adhesive thicknesses to overlayer thickness d. Cracking zones: A, no cracks (safe); B, inner rings (cones), no radials; C, radials, no rings; D, cones and radials; E, radials and outer rings.

$< P_{rad}$); C, radials, no rings ($h > h_*$, $P_{rad} < P < P_{ring}$); D, cones and radials ($h < h_*$, $P_{rad} < P$); E, radials and outer rings ($h > h_*$, $P_{ring} < P$). Thus in applications where it is imperative to remain in the ultra-safe zone A, and especially to avoid radial cracking, the principal requirement is to maintain the adhesive thickness in the region $h \lesssim 0.2d$ as well as to ensure that d [Eqs. (1) and (2)] and r [Eq. (3)] do not become too small. Another requirement is to minimize the incidence of uncommonly large surface flaws, so as to maintain high values of σ_F in Eqs. (1) and (2).

In other applications it may be tolerable to operate in the limited cracking zones B and C, provided the cracks remain wholly contained within the outer brittle layer. In extreme cases where the cracks do traverse the outer layer thickness, the soft adhesive interlayer may act to prevent the cracks from penetrating into the next brittle layer (*cf.* crack penetration in ceramic–metal[27] and ceramic–ceramic[8] multilayers). In dental restorations, for instance, it is clearly desirable to avoid any cracking whatsoever—yet natural teeth sometimes sustain populations of stress cracks (especially in older patients) without immediate failure (although strength is unquestionably degraded). This is true also of car windscreens. In such cases a thick adhesive layer can be beneficial. The separate subject of crack propagation at loads beyond threshold—i.e., the mechanics of transverse crack growth with increasing load to failure—remains to be addressed. In extreme applications such as ceramic armor, where distributed cracking is "encouraged," the multi-cracking zones D and E are preferred.

We close by drawing attention to some issues that might need to be considered in extending the results from our model experiments to more general layer systems:

(i) *Plasticity.* Do the material layers, especially the adhesive, deform entirely within their linear elastic limits? Should we design our layer systems to ensure that this is so, in order to avoid premature subsurface radial cracking? Proliferation of radial cracking has been observed in ceramic–ceramic[10] and ceramic–metal[28] bilayer structures with sublayers of comparable or even higher modulus but lower yield stresses—in those cases it is solely the plasticity that induces the subsurface cracking. In such cases the simple formalism presented in Sec. IV is no longer valid, and it is necessary to resort to numerical (e.g., FEM) computation for analysis.[11,19,29,30]

(ii) *Rate effects.* What is the influence of rate effects in the critical fracture loads? It is implicit in our analysis that the strengths and toughnesses of the glass overlayer are insensitive to chemically-assisted slow crack growth effects; and that the adhesive modulus contains no viscous component. Our justification for ignoring such effects is that we maintained a common crosshead speed throughout our critical load (and strength[19]) tests, so that any such rate effects would "wash" out. Nevertheless, it is arguable that higher crosshead speeds might affect the growth of upper ring cracks more strongly than radial cracks, because of more direct access to atmospheric moisture. Higher crosshead speeds may also result in enhanced stress transfer across the polymeric adhesive interlayer: in glass laminate systems with highly viscoelastic interlayers, such transfer can actually lead to a change in fracture origin from the lower surface of the overlayer to that of the underlayer.[31]

(iii) *Large deflections.* Our relations are based on the notion that the stresses in the overlayer resemble those in a flexing plate on a soft foundation. If deflections are large, membrane stresses may become important.[29,30]

(iv) *Weak interfacial bonding.* If the adhesive bonding is especially weak, delamination may occur, especially during indenter unloading.[18] In layer structures with no bonding at all between overlayer and soft support, the upper layer is free to flex upward at its edges, so diminishing tensile stresses, especially those responsible for the initiation of outer ring cracks.[12]

ACKNOWLEDGMENTS

This work was supported by National Institute of Standards and Technology Guest Scientist funds (Herzl Chai) and a National Institute of Dental Research Grant (PO1 DE10976).

REFERENCES

1. J.E. Gordon, *The New Science of Strong Materials* (Penguin, Harmondsworth, United Kingdom, 1968).
2. W.J. Clegg, K. Kendall, N.M. Alford, T.W. Button, and J.D. Birchall, Nature **347,** 455 (1991).
3. C.A. Folsom, F.W. Zok, and F.F. Lange, J. Am. Ceram. Soc. **77,** 689 (1994).
4. C.A. Folsom, F.W. Zok, and F.F. Lange, J. Am. Ceram. Soc. **77,** 2081 (1994).
5. M.V. Swain and J. Mencik, Thin Solid Films **253,** 204 (1994).
6. D.F. Diao, K. Kato, and K. Hokkirigawa, Trans ASME J. Tribology **116,** 860 (1994).
7. L. An, H.M. Chan, N.P. Padture, and B.R. Lawn, J. Mater. Res. **11,** 204 (1996).
8. H. Liu, B.R. Lawn, and S.M. Hsu, J. Am. Ceram. Soc. **79,** 1009 (1996).
9. A. Pajares, J. Wei, B.R. Lawn, N.P. Padture, and C.C. Berndt, Mater. Sci. Eng. A **208,** 158 (1996).
10. S. Wuttiphan, B.R. Lawn, and N.P. Padture, J. Am. Ceram. Soc. **79,** 634 (1996).
11. A.C. Fischer-Cripps, B.R. Lawn, A. Pajares, and L. Wei, J. Am. Ceram. Soc. **79,** 2619 (1996).
12. T.J. Lardner, J.E. Ritter, and G-Q. Zhu, J. Am. Ceram. Soc. **80,** 1851 (1997).
13. H.M. Chan, Ann. Rev. Mater. Sci. **27,** 249 (1997).
14. K.S. Lee, S. Wuttiphan, X.Z. Hu, S.K. Lee, and B.R. Lawn, J. Am. Ceram. Soc. **81,** 571 (1998).

15. K.S. Lee, S.K. Lee, B.R. Lawn, and D.K. Kim, J. Am. Ceram. Soc. **81,** 2394 (1998).
16. Y.G. Jung, S. Wuttiphan, I.M. Peterson, and B.R. Lawn, J. Dent. Res. **78,** 887 (1999).
17. B.R. Lawn, J. Am. Ceram. Soc. **81,** 1977 (1998).
18. A. Pajares, L. Wei, B.R. Lawn, and C.C. Berndt, J. Am. Ceram. Soc. **79,** 1907 (1996).
19. H. Chai and B.R. Lawn, J. Mater. Res. **14,** 3805 (1999).
20. S. Timoshenko and S. Woinowsky-Krieger, *Theory of Plates and Shells* (McGraw-Hill, New York, 1959), Chap. 8.
21. F.C. Frank and B.R. Lawn, Proc. Roy. Soc. Lond. A **299,** 291 (1967).
22. B.R. Lawn and T.R. Wilshaw, J. Mater. Sci. **10,** 1049 (1975).
23. B.R. Lawn, *Fracture of Brittle Solids* (Cambridge University Press, Cambridge, United Kingdom, 1993), Chap. 8.
24. S.M. Wiederhorn, J. Am. Ceram. Soc. **52,** 99 (1969).
25. B.R. Lawn and A.G. Evans, J. Mater. Sci. **12,** 2195 (1977).
26. B.R. Lawn and D.B. Marshall, J. Am. Ceram. Soc. **62,** 347 (1979).
27. M.C. Shaw, D.B. Marshall, M.S. Dadkhah, and A.G. Evans, Acta Metall. **41,** 3311 (1993).
28. H. Zhao, X.Z. Hu, M.B. Bush, and B.R. Lawn, J. Mater. Res. **15,** 676 (2000).
29. K. Komvopolous, ASME J. Tribology **111,** 340 (1989).
30. P. Montmitonnet, M.L. Edinger, and E. Felder, ASME J. Tribology **115,** 15 (1993).
31. S.J. Bennison, A. Jagota, and C.A. Smith, J. Am. Ceram. Soc. **82,** 1761 (1999).